JOURNAL OF MATERIALS SCIENCE 10 (1975) 1626–1635

Creep-compensated fatigue testing of polyethylene under reversed loading conditions

J. W. TEH, J. R. WHITE,* E. H. ANDREWS
Department of Materials, Queen Mary College, University of London, UK

A machine capable of testing polymers under creep-compensated strain-controlled cyclic deformation has been constructed, and used initially to study fatigue behaviour in low-density polyethylene. Reversed loading conditions have been used with total strain amplitude up to 6.5%. Crack propagation is inhibited by the compressive component of the deformation. Within the range of testing employed, the slowest crack-growth rates are obtained for a particular tensile amplitude when the compressive component is such that minimal accumulated dynamic creep is measured.

1. Introduction

The conditions which promote fatigue failure in a polymeric material are quite different from those attaching to a metallic component of similar dimensions. Testing equipment developed for the study of metals is, consequently, of limited value in the investigation of polymers, although modifications can sometimes be made to improve its suitability [1-5]. The stresses required to promote fatigue failure in polymers are generally much smaller than those for metals, while deformations can be much larger. The thermal conductivity of a polymer is insufficient to cope with the plastic or visco-elastic energy dissipation unless frequencies are less than about 2 Hz; catastrophic temperature rises occur if testing is attempted at frequencies commonly used in metal studies [6-8]. Finally, polymeric samples may creep significantly under cyclic loading conditions [3, 9-14]. Therefore, it is important either to measure the accumulated creep periodically and assess its significance when interpreting the data, or to arrange the test procedure so that creep is continuously monitored and appropriate compensation introduced into the deformation cycle [10, 15]. More detailed discussion of the fatigue testing of polymers is to be found elsewhere [9, 10, 16].

The work presented here represents part of a study conducted on a machine designed specifically for polymer fatigue tests. The current series of experiments involves compression–tension cycling, thus extending earlier work performed in tension only [10]. A description of the machine in its present form is included and indication made of those modifications showing significant departure from the original design used in the tensile cycling studies [10, 17].

2. The test machine

2.1. The specimen drive

A schematic diagram of the machine is shown in Fig. 1. The dumb-bell specimen, A, is strained by link B which is moved by the rocking motion of lever C; the lever is pivoted at D and driven by a pin on a crank table sliding in the slot E. When the crank table is rotating at a constant velocity

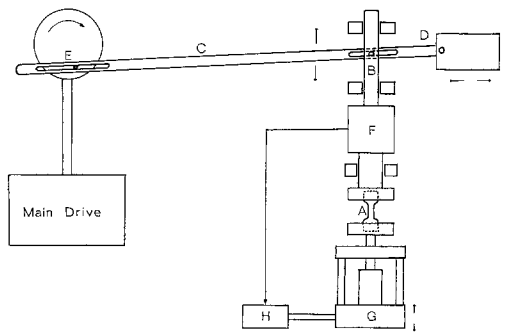

Figure 1 Schematic representation of the testing machine. (See text for key.)

*Present address: Department of Metallurgy and Engineering Materials, University of Newcastle upon Tyne, UK.

the pin describes a motion which has a sinusoidal component in the direction perpendicular to the mean position of the lever (i.e. in the direction of the motion of link B). Since the co-ordinate of the pin along the lever varies, however, the displacement of a point on the lever is not truly sinusoidal. A simple formula for the true profile in terms of the radial position of the pin on the crank table and the length of the lever shows that, for the geometry employed, the assumption of a sinusoidal displacement is, nevertheless, true to within 2% at all points in the cycle for even the largest amplitudes available.

There are fifteen sites for the pin at different radii on the crank table, providing coarse adjustment of displacement amplitude, while intermediate amplitudes can be obtained by varying the position of the pivot, D, a continuous adjustment which may be employed during operation if so desired. The range of amplitude available at present is $\pm$ 0.125 mm to $\pm$ 7.50 mm, with a corresponding deflection range of 0.25 to 15.0 mm when operating in tension only or compression only.

The crank table is driven by a three-phase, $\frac{1}{2}$ hp motor-gearbox unit operating through a secondary gearbox, this combination giving a range of output cycling rates between 41 and 0.667 cycles per minute. The chasis consists of a girder frame, welded to the top of which are two flat plates. On one of these is mounted the primary drive and on the other the operating mechanism. The operating mechanism sub-assemblies are all dowelled to the plate, so that they can be removed and replaced without upsetting the alignment. The chassis is bolted to a table through six anti-vibration mounts.

The advantages of mechanical reliability, reproducibility and range of frequency and amplitude offered by this simple drive arrangement were considered to outweigh any simplification in interpretation which might result from the use of a constant deformation rate as opposed to a sinusoidal strain cycle.

2.2. Load measurement

The non-driven end of the specimen is rigidly coupled to a Pye-Ether UF-2 transducer capable of measuring both tensile and compressive loads up to 90 N, with a displacement of 0.45 μm N^{-1}; this is negligible compared to the motion of the driven end for the materials under examination. The load cell is mounted on a rigid supporting frame (at G in Fig. 1), which is normally held stationary but can be moved in guides parallel to the axis of the test piece to compensate for creep. This movement occurs by the action of a micrometer screw driven by a servomotor which is activated whenever specimen creep is detected, (see Section 2.4). The output signal of the load transducer is applied to the "Y" channel of an X-Y recorder.

The load measuring device described above replaced an earlier deflecting beam apparatus used by Andrews and Walker [17]. The performance of this arrangement under the higher amplitude and reversed loading conditions of the present investigation was found to be unsatisfactory, probably due to frictional opposition to smooth bending at the beam support columns.

2.3. Deformation measurement and strain determination

The driven end of the specimen clamp is connected to a linkage lever which magnifies the displacement. The movement of the driven end is thus measured instantaneously by a Pye-Ether PD12 linear resistance transducer attached to the remote end of the linkage lever, and the output fed to the "X" side of the X-Y recorder. This signal is calibrated for the strain suffered within the gauge length by comparing with the displacement of markers measured by a photographic technique in a separate series of static deformations.

2.4. Dynamic creep compensation

The method for dynamic creep compensation is based on a set of microswitches arranged to continuously test for the occurrence of permanent deformation (due to creep), at the zero stress points in the cycle. When dynamic creep is detected, compensation is achieved automatically by the activation of a servomotor which drives the rigid frame, G, to which the non-driven end of the specimen is connected, through the load transducer (Section 2.2).

A schematic cross-section of the arrangement is shown in Fig. 2. The driven end of the specimen is clamped tightly in a block, F_1, connected to a piston, F_2, which rides in a cylinder, F_3. The cylinder, F_3, is attached rigidly to the reciprocating link, B. The motion of this link is transferred to the specimen via the piston, F_2, in one of two ways. To compress the specimen, with B moving to the left, face a_1 of the reciprocating link makes contact with face a_2 of the piston, and

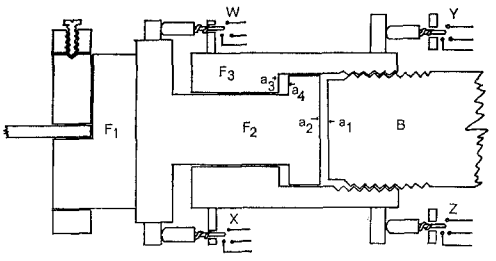

Figure 2 The load application device, showing the decoupled state.

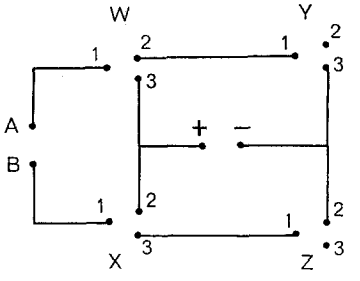

Figure 3 Creep compensation control switching. The switches have two modes: in the "operating", (switch depressed) condition terminals 1 and 2 are connected, terminal 3 is isolated. In the "reset" position, terminals 1 and 3 are connected, terminal 2 is isolated. A single power supply is used and the sense of the signal fed to the motor determines its sense of action. The power supply cannot be short circuited using the above arrangement, even when the switch positions are maladjusted.

drives it to the left. To extend the specimen, with B moving to the right, the deep ledge on the inside of cylinder F_3 at a_3 catches upon the enlarged head, a_4, of the piston F_2, and pulls it to the right. The pairs of faces at a_1, a_2 and at a_3, a_4 are constructed to be accurately parallel to prevent jerky pick-up on passing from the compression half-cycle to tension, and vice versa.

Cylinder F_3 is attached to the reciprocating link by means of a screw thread, so that the distance between a_3 and a_1 is adjustable. Hence for tests involving tension/compression cycling the specimen can be decoupled from the driving motion for a controlled fraction of each half cycle. In a typical tension/compression test the machine is set up so that this unstressed condition occurs at the central zero of displacement of the reciprocating link. The strain profile remains nearly sinusoidal even when the drive is decoupled for a substantial fraction of each half-cycle (see Appendix).

Microswitches Y and Z, activated by a stiff bar moving with the reciprocating link, are arranged so that for the compression half-cycle connections Y1-Y3 and Z1-Z3 are made, while for the tension half-cycle connections Y1-Y2 and Z1-Z2 are made (see Fig. 3 for circuit diagram). Microswitches W and X probe the motion of the driven end of the specimen so that for the compression half-cycle connections W1-W3 and X1-X3 are made, (except during a small adjustable fraction near to the onset of this half-cycle) and for the tension half-cycle connections W1-W2 and X1-X2 are made (apart from a small adjustable fraction). When the specimen is unstressed W will normally have terminals W1-W2 connected, and X will have X1-X3 connected.

Suppose, however, creep occurs, and let us consider in particular the case where creep in the tension half-cycle dominates, i.e. we obtain a "permanent" extension of the specimen. This will cause the face a_2 to get progressively nearer to face a_1 at the zero point of the motion. When sufficient extension has accumulated, switch W will have terminals 1 and 3 connected before switch Z operates, on moving from extension to compression. This condition clearly indicates creep in extension has occurred, and in this state the circuit activates a relay to switch on the servomotor and causes a retraction of the non-driven end of the specimen, increasing its distance from the mean position of the driven end.

A similar situation occurs if compression creep dominates, but this time the servomotor is activated by a signal of opposite polarity, and moves the non-driven end of the specimen closer to the driven end.

The relay switches which operate the servomotor are connected with time-delay devices which allow driving to be prolonged for a prefixed time interval ($\frac{1}{4}$, $\frac{1}{2}$ or 1 sec) after the signal current terminates. This is necessary at the beginning of tests run at the highest frequencies and high strain amplitudes, where the short decoupling time is insufficient for the servomotor to counteract all the creep induced during the previous half cycle.

The positions of switches W, X, Y, Z are all independently adjustable so that the total accumulated creep deformation required before the compensation adjustment is activated can be controlled. The microswitches employed are Burgess type CR1 in conjunction with CQ1

activators to provide for the required overtravel. They are rated as having a maximum "movement differential" (i.e. separation between operating position and release position) of 0.025 mm. Used in the manner described here the movement differentials of any pair of switches tend to cancel, however, and a switching precision better than this value is possible with careful adjustment.

The total accumulated creep is, of course, the total movement of the rigid frame carrying the load transducer, and this is measured by a sensitive dial gauge. A correction equal to half the "free run" on decoupling has to be added to this value to account for the initial take up of slack.

2.5. Tension only/compression only testing

The machine was initially required for tests in tension only [10] and incorporated an earlier design for the specimen clamp/decoupling system [17]. The arrangement was, however, exactly equivalent to that obtained with the current design when the specimen is set to zero strain at one extreme of the cycle. Consequently, the specimen is in tension throughout the cycle with the exception of a short, adjustable period of decoupling at this extreme during which creep detection and compensation occurs as before.

Similarly, if compression-only testing is required, it is necessary only to introduce the sample such that the zero strain position occurs at the opposite extremity of the cycle to that described for tension-only testing.

2.6. Environmental chamber

An "open circuit" air circulating system is used to maintain constant temperature around the specimen. Compressed air is passed over a heating/cooling coil and into the specimen enclosure to exhaust through vents. "Perspex" walls and top permit observation of cracks, and the enclosure is illuminated by a bulb which can be positioned for optimum lighting conditions during a test without disturbing the specimen enclosure. Thermostatic control of the enclosure temperature is achieved by adjusting the heating coil current by means of an Ether-type 12-92 controller.

2.7. Measurement of crack-growth rates

Crack-front positions are recorded at frequent intervals using a travelling microscope with micrometer eye piece. The difference, Δc, between successive measurements separated by an interval ΔN ($\sim$ 50), gives an average growth rate dc/dN at $N + \Delta N/2$. Cracks are initiated by pressing a previously unused razor blade into the sample, to produce a central edge crack with a vertical crack front.

3. Experimental

The material used was ICI low density polyethylene (LDPE) type WJG11, (density = 0.918 $\times$ 10^3 kg m^{-3}; MFI = 2.0). Sheets 4 mm thick were compression moulded directly from granules at 160°C under a pressure of 100 MN m^{-2} and then rapidly cooled. Dumb-bell shaped specimens were stamped out and placed in a male/female mould to be compressed to the required thickness of 3 mm at 120°C and then air-cooled (Fig. 4). This test piece configuration replaces the one used by Andrews and Walker which is prone to buckling if used in compression. Specimens were allowed to age at room temperature for six weeks prior to testing.

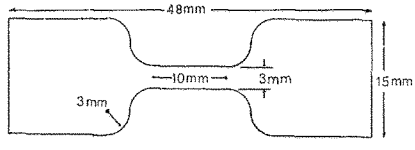

Figure 4 Plan of the test piece, (depth 3 mm at all points); all radii are 3 mm.

The tests detailed below employed razor-notched samples and were conducted at 293 or 298 K using a driving frequency of 0.25 Hz.

4. Results

4.1. The deformation cycle

A typical load-deformation cycle characteristic is shown in Fig. 5; considerable hysteresis is evident. The material is stiffer in compression than in tension with the peak stress in compression always greater than that in tension for symmetrical straining experiments. A feature peculiar to the mode of operation described here is the short horizontal portions (P_1P_2, $P'_1P'_2$) on the zero load axis. These correspond to recovery which occurs during the decoupled parts of the cycle. There is insufficient time for recovery to zero strain (as has been found to occur in LDPE given sufficient time [18]), and a residual creep strain remains at the beginning of the next (reversed) loading. It would be unrealistic to attempt to compensate for this

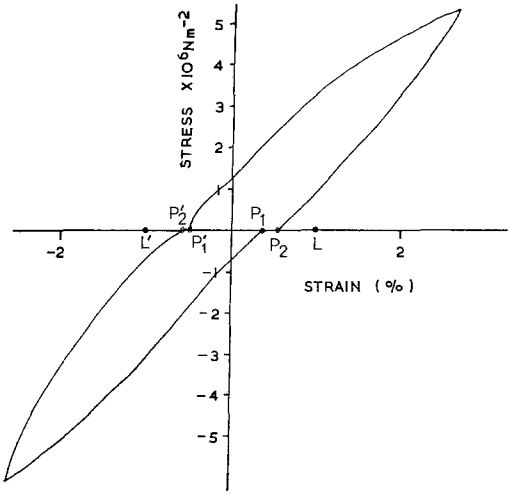

Figure 5 Stress–strain characteristic obtained near the beginning of a test.

since the effect of the deformation half cycle which follows is to remove it and produce creep in the opposite sense. The creep detection mechanism is hence set to operate at positions slightly further out than the limits P_2, P'_2 – say at L and L′. If the net creep per cycle is not exactly zero, so that the hysteresis loop is not exactly closed, then the characteristic will shift to the left or right. If, for example, tensile creep is dominant, the characteristic will continue to the right each cycle, and eventually P_2 will reach L and the creep compensation mechanism will be activated.

4.2. Fatigue data

Although care was taken to standardise the depth of the razor cut, the precision achieved was considered to be inadequate with respect to fatigue lifetime in view of the major contribution to the total of "stage 1" of the fatigue growth, when the crack is short and the rate of propagation very small [10, 17]. Consequently, we have chosen to present "fatigue life" data in terms of the number of cycles, N_f, for a crack to grow from 0.8 to 2.0 mm. The number of cycles to reach 0.8 mm (dependent partly on the initiation depth), has hence been ignored even when significant. The choice of failure criterion (i.e. a crack length of 2.0 mm) is probably more realistic than complete severance, as serious necking and rapid crack growth usually occur soon after attainment of this condition.

Reversed loading tests were carried out for three values of total strain, ϵ_T, defined as

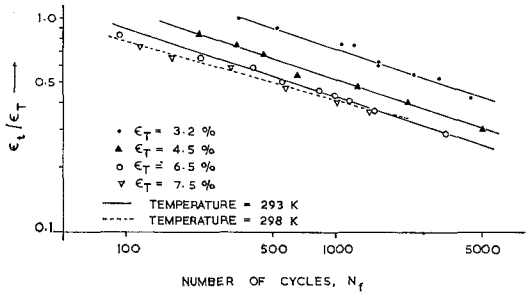

Figure 6 Effect of strain range and temperature. The ratio of the tensile component of strain, ϵ_t, to the strain range, ϵ_T, is plotted against the number of cycles, N_f, required to propagate a crack from 0.8 to 2.0 mm in length for three different values of ϵ_T at 293 K and one at 298 K.

$$\epsilon_T = |\epsilon_c| + |\epsilon_t|$$

where ϵ_c and ϵ_t are the maximum strains in compression and tension respectively. The values chosen for ϵ_T were 6.5%, 4.5% and 3.2%. The ratio ϵ_c/ϵ_t was varied and the effect on the lifetime, (as defined above) is shown in Fig. 6. The linear plots may be approximated by the empirical relationship

$$\log(\epsilon_t/\epsilon_T) = A(\epsilon_T) + B \log N_f \qquad (1)$$

where B is a constant. The negative slope of lines of constant ϵ_T shows that increased lifetime results when ϵ_t is reduced (ϵ_c will increase by an equal amount). That is, increasing the compressive component increases the lifetime in fixed strain amplitude testing.

The effect of introducing a compressive component into the deformation cycle could alternatively be demonstrated by means of a three-dimensional plot with cartesian axes ϵ_t, ϵ_c and N_f. A simpler two-dimensional representation has been employed, following a suggestion by Gough [19] (Fig. 7). Contours of constant fatigue life (as defined above) are constructed on a graph in which the value of ϵ_c for each test is plotted against the corresponding value of ϵ_t. Fatigue behaviour at constant ϵ_t, constant ϵ_c, constant ϵ_T (represented by a line of gradient unity) or constant mean strain (represented by a line of slope -1), can be readily deduced from this diagram. The most significant result derives from the fact that all of the contours curve away from the ϵ_c axis. Hence for a constant tensile strain, ϵ_t, the fatigue life is improved by increasing the strain in compression, ϵ_c, at least within the range of testing reported here. The contours shown in Fig. 7 were obtained as follows.

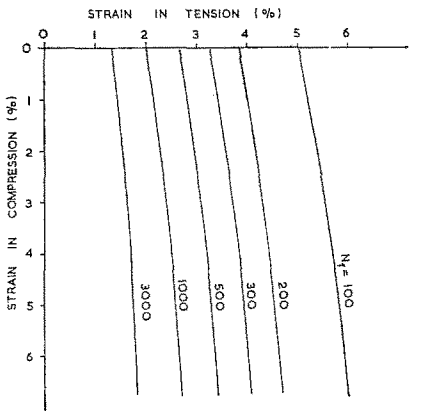

Figure 7 Contours of constant N_f showing a marked difference in behaviour with respect to changes in the tensile and compressive components of strain respectively.

Assume that for $\epsilon_c = 0$, the fatigue life, N'_f is related to $\epsilon_T (= \epsilon_t)$, by an expression of the form [20]

$$\log \epsilon_T = C + D \log N'_f . \quad (2)$$

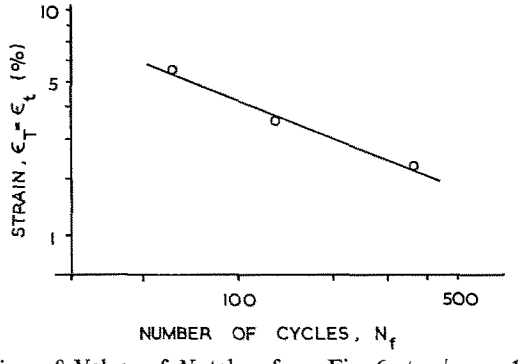

Figure 8 Values of N_f taken from Fig. 6 at $\epsilon_t/\epsilon_T = 1$, (≡ tension-only testing), for the 293 K characteristics.

Fig. 8 was constructed from values of N'_f read from Fig. 6 at the points of intersection of the characteristics corresponding to the three different values of ϵ_T and the horizontal line $\epsilon_t/\epsilon_T = 1$. For this condition, Equation 1 becomes

$$\log 1 = 0 = A(\epsilon_T) + B \log N'_f \quad (3)$$

$$\therefore \log \epsilon_t/\epsilon_T = B \log N_f/N'_f . \quad (4)$$

On substituting for N'_f using Equation 2, and replacing B, C and D by values taken from Figs. 6 and 8, Equation 4 is replaced by the empirical relationship

$$\log \epsilon_t/\epsilon_T = -0.32 \log N_f - \frac{(1.5 - \log \epsilon_T)}{0.4} . \quad (5)$$

This equation which is, of course, applicable only to the data under scrutiny, was used to generate the contours shown in Fig. 7. By re-arrangement and differentiation of Equation 5, it can be shown that $dN_f/d\epsilon_c$ is always positive for any fixed value of ϵ_t, confirming the beneficial effect of compression deduced from the graphical presentation.

4.3. Effect of temperature

Most of the tests have been conducted at 20°C, but a limited series of experiments have been performed to investigate the importance of temperature control. Even increasing the specimen enclosure temperature to 25°C produces a significant difference, as can be seen on reference to Table I in which the results shown in Fig. 6 are summarized.

TABLE I

Temperature (°C)	ϵ_T (%)	B	Standard error on B	Effective frequency (Hz)
20	3.2	−0.336	±0.024	0.35
20	4.5	−0.330	±0.017	0.33
20	6.5	−0.309	±0.018	0.30
25	7.5	−0.268	±0.014	0.30

The values of the gradient, B (Equation 1), and the standard errors are calculated using a least squares analysis. The results at 20°C are consistent with the hypothesis that B is independent of ϵ_T, but a significant difference is found at 25°C. A detailed study of the effect of temperature is reserved until later, but it is clear that strict control of temperature is necessary if meaningful data are to be recorded.

4.4. Creep data

Typical examples of accumulated creep measurements plotted against the number of deformation cycles are shown in Fig. 9. For the test conditions shown so far, creep is positive when $|\epsilon_c| \geqslant 1.7 |\epsilon_t|$ while the rate increases monotonically with $|\epsilon_t - \epsilon_c|$ for a particular ϵ_T. Creep is negligible when $|\epsilon_t| \sim |\epsilon_c|$; this result is not as insignificant as it may at first seem, since the corresponding stresses are by no means equal, due to the relative ease of extension compared to compression. The onset of measur-

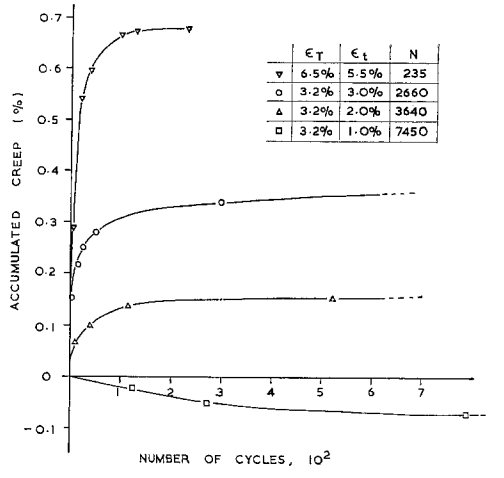

Figure 9 Accumulated creep for three tests with ϵ_T = 3.2%, showing the effect of changing ϵ_t. Results from a test conducted at a much higher strain are also shown.

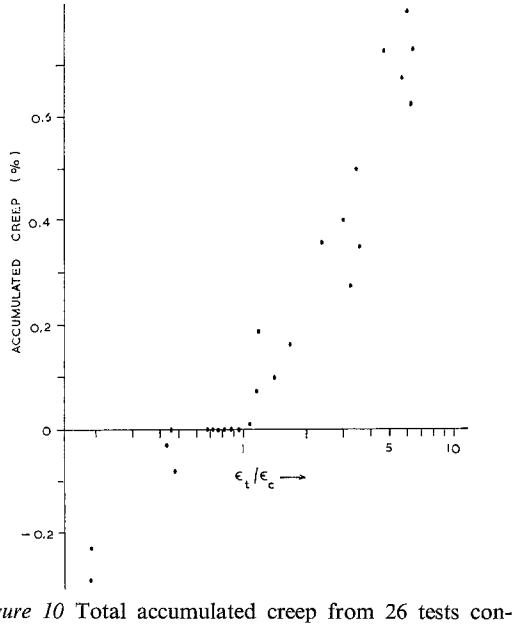

Figure 10 Total accumulated creep from 26 tests conducted under different strains, displayed against ϵ_t/ϵ_c. Note that for $0.6 < \epsilon_t/\epsilon_c < 1.0$ creep cannot be detected within the precision of the experiment.

able creep in compression seems to be delayed until $\epsilon_c \sim 1.7\epsilon_t$ on increasing ϵ_c relative to ϵ_t (Fig. 10).

4.5. Crack growth data

The application of fracture mechanics to the study of fatigue in polyethylene, based on crack-growth rates measured using the machine for tension only cycling, has already been discussed [10]. A subsequent paper will deal with the data from reversed loading tests.

5. Discussion

Before commenting on the implications of the results of this investigation, the reader is reminded of the somewhat arbitrary definition of fatigue life employed here, which should more properly be described as "that contribution to the total fatigue life accrued during propagation of the crack from 0.8 to 2.0 mm". No illumination is offered on the influence of compressive loading on crack initiation at this time.

Two important facts have emerged from the preliminary studies presented above.

(a) The introduction of a compressive component into the deformation cycle appears to be advantageous whether working under conditions of a fixed strain amplitude (ϵ_T) or with a fixed tensile strain (ϵ_t). This seems to indicate that at least some of the damage which occurs during tensile deformation is reversed by subsequent compression. This is an interesting result since there is no *a priori* reason why structural changes produced during compression should be of this nature rather than a preparation for enhanced crack growth.

The benefit gained when working with a fixed strain amplitude is at first sight in contradiction to the results of Yamada and Suzuki [21] who find that increasing the mean tensile stress promotes improved fatigue lifetime. Their tests are conducted wholly in tension, however, and do not anticipate behaviour under the influence of compression. There is hence insufficient ground for a detailed comparison, and it may also be significant that their tests were conducted under load-controlled conditions while the experiments described above were strain-controlled and creep-compensated. It is interesting to observe, however, that if the data of Yamada and Suzuki and that presented here are taken together, it appears to be indicated that for a particular strain range, the shortest fatigue life will occur when the component is cycled in tension with the minimum strain near zero. Such conditions are very common in practice.

Immediate cross comparison of results of the current investigation with those of Andrews and Walker [10] are frustrated by the different geometries of the test pieces. An attempt to overcome this difficulty by comparing tests operated under similar values of W_0, the elastic stored energy density, remote from the crack, has

revealed that crack propagation is faster in tensile-only tests than in reversed loading with similar (peak) W_0 in tension.

(b) Introduction of compression reduces the net accumulated creep. At this stage it is impossible to deduce whether microscopic changes associated with tensile creep are actually reversed, (totally or partially), or whether different, yet compensating, changes occur. The balance of compressive and tensile components in the deformation cycle producing minimal (negligible) dynamic creep seems to be achieved concurrently with the minimum crack propagation rate. This implies that at least some of the damage is reversible. More important in the practical sense is that stress conditions producing maximum dimensional stability (minimum creep) coincide with those yielding a high fatigue life.

Tests are in progress to explore the range of conditions over which these statements hold true.

6. Conclusions

The results of the current study illustrate the value of introducing creep compensation into the fatigue test of a polymer. A more detailed specification of the optimal loading characteristics of a component can be derived. The test machine has proved capable of high precision control and monitoring of the tests, and experiments currently in progress will be described in a subsequent publication.

Appendix: Strain profile suffered by the specimen in compression/tension testing

The creep compensation adjustment requires that the specimen is decoupled from the driving mechanism each half-cycle, such that the strain profile of the specimen cannot be inferred directly from the motion of the reciprocating link. This can be seen on reference to Fig. 11. The motion of the link is closely sinusoidal, as a result of the arrangement from which it derives, and can be represented by

$$y = A \sin \frac{2\pi t}{T} \tag{6}$$

where T is the period and A the amplitude.

Consider first the case where $|\epsilon_c| = \epsilon_t$. If no specimen creep has occurred, the part of this motion transferred to the specimen is that above $y = B$ plus that below $y = -B$(Fig. 11a), where

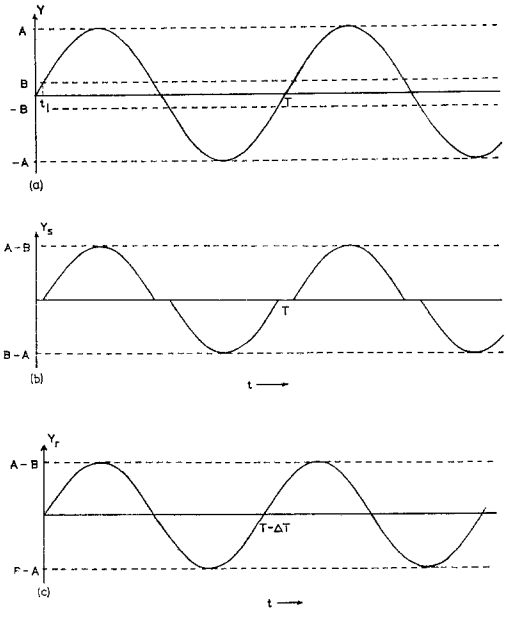

Figure 11 (a) Motion of the link. The displacement parallel to the axis of the specimen is plotted as y. (b) Motion transferred to the driven end of the specimen, on taking account of decoupling. (c) Reduced deformation cycle.

$y = B$ corresponds to the position in the tensile portion of the motion at which the specimen becomes engaged, and $y = -B$ is the corresponding position in the compressive half-cycle.

Suppose the total "dead" time (or decoupled time) per cycle is ΔT. Then the time, t_1, at which the specimen first becomes engaged is $\Delta T/4$, whence

$$B = A \sin \frac{\pi \Delta T}{2T} \cdot \tag{7}$$

Consequently, the deformation, Y_s, suffered by the specimen can be described as follows:

$$\left.\begin{aligned} &\frac{nT}{2} - \frac{\Delta T}{4} < t < \frac{nT}{2} + \frac{\Delta T}{4} \\ &\text{for } Y_s = 0; \\ &\frac{nT}{2} + \frac{\Delta T}{4} < t < \frac{(n+1)T}{2} - \frac{\Delta T}{4} \\ &\text{for } Y_s = A \sin \frac{2\pi t}{T} - B \\ &\quad = A \left\{ \sin \frac{2\pi t}{T} - \sin \frac{2\pi}{T} \frac{\Delta T}{4} \right\} \cdot \end{aligned}\right\} \tag{8}$$

This function is shown in Fig. 11b.

If we now choose to ignore any changes which occur in the specimen during the "dead" time, we can re-plot this function as in Fig. 11c. This function has period $(T - \Delta T)$, amplitude $(A - B)$, and can be represented over the first half-cycle by

$$Y_r = A\left\{\sin\frac{2\pi}{T}\left(t + \frac{\Delta T}{4}\right) - \sin\frac{2\pi}{T}\frac{\Delta T}{4}\right\}. \quad (9)$$

We will now compare this profile with the sinusoidal displacement having the same period and amplitude, i.e.

$$Y_h = (A - B)\sin\frac{2\pi t}{T\text{-}\Delta T}$$

$$= A\left\{1 - \sin\frac{2\pi}{T}\frac{\Delta T}{4}\right\}\sin\frac{2\pi t}{T - \Delta T}. \quad (10)$$

Put

$$E = \frac{Y_h}{Y_r}$$

$$= \frac{(1 - \sin[(2\pi/T)(\Delta T/4)])\sin(2\pi t/T - \Delta T)}{\sin(2\pi/T)[t + (\Delta T/4)] - \sin[(2\pi/T)(\Delta T/4)]}.$$

By using differential calculus to locate the extrema of $E(t)$, and simplifying by assuming that ΔT is sufficiently small to make $(\Delta T/T)^2$ negligible, it can be shown that the value of E furthest from unity occurs close to $t = T/6$. E is a slowly changing function, so we can evaluate for this position to find

$$E_{min} \simeq 1 - 0.06\frac{\Delta T}{T}.$$

If we require that this differs from unity by less than $P\%$, then

$$0.06\frac{\Delta T}{T} < \frac{P}{100}$$

$$\therefore \frac{\Delta T}{T} < \frac{P}{6},$$

e.g. if we insist that the profiles match to within 2% at all points then

$$\frac{\Delta T}{T} < 0.33.$$

This condition should not be too difficult to achieve in practice.

Conversely, suppose $\Delta T/T < 0.3$ then $P < 1.8\%$. The corresponding "dead" distance is

$$2B = 2A\sin\frac{\pi}{2}\frac{\Delta T}{T} \simeq 0.9A.$$

A similar calculation shows that an analogous transformation can be applied to non-symmetric cycling, together with a vertical shift (relative to the $y = 0$ axis).

The function shown in Fig. 11c has a frequency $fT/(T - \Delta T)$ where f is the frequency corresponding to Fig. 11a. This "effective frequency" has been recorded in Table I, but it has not yet been established which value, (i.e. f or $fT/(T - \Delta T)$ is more appropriate to characterise tests conducted under the conditions employed here.

Acknowledgements

This work is financed by the Science Research Council. J. W. T. acknowledges the University of Science of Malaysia for support through the ASTS Fellowship scheme.

References

1. J. P. ELINCK, J. C. BAUWINS and G. HOMÈS, *Int. J. Fract. Mech.* **7** (1971) 277.
2. R. W. HERTZBERG, H. NORDBERG and J. A. MANSON, *J. Mater. Sci.* **5** (1970) 521.
3. S. ARAD, J. C. RADON and L. E. CULVER, *J. Mech. Eng. Sci.* **14** (1972) 328.
4. J. S. HARRIS and I. M. WARD, *J. Mater. Sci.* **8** (1973) 1655.
5. A. S. ARGON and D. G. BAILEY, *ibid* **9** (1974) 201.
6. R. J. CRAWFORD and P. P. BENHAM, *ibid* **9** (1974) 18.
7. L. J. BROUTMAN and S. K. GAGGAR, *Int. J. Polym. Mater.* **1** (1972) 295.
8. I. CONSTABLE, J. G. WILLIAMS and D. J. BURNS, *J. Mech. Eng. Sci.* **12** (1970) 20.
9. E. H. ANDREWS, in "Testing of Polymers", Vol. 4, edited by W. E. Brown (Wiley, New York, 1969) p. 237.
10. E. H. ANDREWS and B. J. WALKER, *Proc. Roy. Soc. Lond.* **A325** (1971) 57.
11. H. F. BORDUAS, L. E. CULVER and D. J. BURNS, *J. Strain Anal.* **3** (1968) 193.
12. A. R. BUNSELL and J. W. S. HEARLE, *J. Mater. Sci.* **6** (1971) 1303.
13. *Idem, J. Appl. Polymer Sci.* **18** (1974) 267.
14. N. H. WATTS and D. J. BURNS, *Polymer Eng. and Sci.* **7** (1967) 90.
15. A. R. BUNSELL, J. W. S. HEARLE and R. D. HUNTER, *J. Phys. E.* **4** (1971) 868.
16. S. RABINOWITZ and P. BEARDMORE, *J. Mater. Sci.* **9** (1974) 81.
17. B. J. WALKER, Ph.D. Thesis, University of London (1969).
18. G. H. EDWARD and E. H. STACHURSKI, *J. Phys. D.* **7** (1974) 1778.
19. W. A. GURNEY and I. C. CHEETHAM, *Trans. I.R.I.* **35** (1959) 45.

20. S. S. MANSON and M. H. HIRSCHBERG, Proceedings of the 10th Sagamore Army Materials Research Conference (Syracuse University Press, Syracuse, New York, 1964) p. 133.
21. K. YAMADA and M. SUZUKI, *Kobunshi Kagaku* **30** (1973) 206; (English translation, *Kobunshi Kagaku* **2** (1973) 349).

Received 22 November 1974 and accepted 6 February 1975.